Receiver Alignment Dependence of a GA Controlled Optical Wireless Transmitter

M D Higgins, R J Green and M S Leeson

School of Engineering, University of Warwick, Coventry, CV4 7AL, UK

E-mail: m.higgins@warwick.ac.uk, roger.green@warwick.ac.uk, mark.leeson@warwick.ac.uk

Abstract. A genetic algorithm controlled multispot transmitter is demonstrated to be capable of optimising the received power distribution for single element receivers in fully diffuse mobile indoor optical wireless systems. By dynamically modifying the intensity of individual diffusion spots, the transmitter is capable of compensating for changes in receiver alignment, user movement and surface reflectivity characteristics, with negligible impact to bandwidth and RMS delay spread. The dynamic range, referenced against the peak received power, can be reduced by up to **27%** when the room is empty, and up to **26%** with user movement and variable receiver alignment. Furthermore, received power perturbation, induced by user movement, is reduced from **10%** to **2.5%**. This method shows potential for providing a highly adaptable solution of overcoming channel variability whilst also reducing receiver complexity.

Keywords: Genetic algorithm, optical communication, wireless LAN.

Submitted to: *J. Opt. A: Pure Appl. Opt.*

1. Introduction

Indoor optical wireless (OW) communication systems using an infrared (IR) carrier combine the high bandwidth availability of the optical domain with traits of mobility found in their radio frequency (RF) counterparts [1]. Coupling these features to form a high performance system requires the overcoming of the limitations imposed by the transmission channel, for which the characteristics are dependent upon the room size, stationary and moving objects, material properties of every surface the radiation is incident upon, and the number and type of illumination sources present [2]. This, essentially infinite, level of channel variability implies a single system design may have different performance capabilities when deployed in different environments.

Several solutions have been proposed for mitigating the channel's influence on system performance. Quasi-diffuse configurations employing multispot diffusion (MSD) and diversity receivers [3], ameliorate the bandwidth and ambient noise rejection through the use of an array of photodetectors coupled to either a single imaging lens [4], or several optical concentrators [5]. Modulation techniques, such as trellis-coded pulse-position modulation [6], and amplitude shift key digital demodulation [7] are capable of overcoming the effects of intersymbol interference (ISI), and cyclostationary noise from fluorescent lamps [8], respectively. The use of *intelligent* techniques have also been shown to be beneficial, using neural networks and pattern recognition wavelet analysis to overcome channel induced distortion [9]. Following this, a modified genetic algorithm (GA), based on simulated annealing [10], has been shown to produce highly optimised computer generated holograms, reducing the variation in received power distribution [11, 12].

OW systems are typically employed with a cellular architecture, where a room or section of a room, has a transceiver base station linking multiple battery powered OW receivers to the backbone network. Therefore, whilst certain performance merits can be attributed to each of the aforementioned techniques, the increased cost, complexity and physical size of each receiver deployed must be considered. This will become especially apparent when the number of receivers becomes large, as the cost and/or complexity overhead of a system will be influenced more by the number of receivers, than a single base station.

Recently, work was proposed based upon a GA controlled MSD transmitter, but where the traditionally employed diversity receiver was replaced with a simpler single element receiver [13, 14]. Using the GA to control the intensity of individual diffusion spots, similar received power distributions, with negligible impact on bandwidth and RMS delay spread, could be formed in multiple rooms independent of the reflectivity characteristics and user movement patterns. The adaptability provided the possibility of implementing a simpler receiver, as the transmitter became responsible for overcoming channel variability. The study was conducted and proposed as a 'proof of concept', with the aim of understanding, applying and quantifying the feasibility and effectiveness of the GA approach. Simplifications were made to the system model, one of which

in particular, was that all receivers where orientated towards the ceiling, even whilst moving.

It has to be assumed that users of OW systems are aware that some level of transmitter-receiver alignment must exist to take advantage of larger bandwidth availability compared to a RF system where freedom of movement is invariably higher. However it is the system designer who defines and furthermore imposes upon the end user the alignment criteria as an operational requirement. A balance must be found between system performance and user-friendliness. In this paper the effectiveness of the GA is investigated with the incorporation of variable receiver alignment to the already established model that includes user movement in multiple environments. The results establish the relationships between receiver FOV and GA performance, and the increased level of user freedom the GA can provide for applications where cost, connectivity and user mobility are paramount.

The remainder of this paper is organised as follows. Section 2 overviews the general system model and impulse response calculations. Section 3 introduces the channel model theory followed by section 4 that covers the GA implementation. Section 5 provides the results and associated analysis followed by concluding remarks in section 6.

2. System Model

2.1. Source, Receiver and Reflector Model

We define our system environment to be an arbitrary indoor rectangular room for which the majority of surfaces exhibit a fully diffuse reflection characteristic that can be described by Lambert's reflection model [15]. A diffusion spot geometry is formed using either multiple optical sources [16], or a 2-D array of either vertical cavity surface emitting Laser diodes (VCSELs) or resonant cavity LEDs (RCLEDs), flip-chip bonded to CMOS driver circuitry [17, 18]. For the case of multiple optical sources the radiation profile can be controlled via lenses or other diffuser techniques [19], but typically the source is an LED which emits radiation with a generalised Lambertian radiation intensity pattern [20]. Therefore, from a receiver point of view, if both LEDs and the reflected radiation from a 2-D VCSEL/RCLED array appear simply as sources exhibiting a Lambertian radiation intensity pattern, we can make a model simplification, that from this point onwards, each of the I diffusion spots on the ceiling will be considered independent sources $\mathcal{S}_i$. The only error induced with this assumption is a delay and propagation loss between the emitting element of a 2-D VCSEL/RCLED array and the diffusion spot position. However, this assumption also allows us to simplify our argument for using the GA, whilst maintaining generality to the application independent of the technique used for diffusion spot generation.

Referring to figure 1, each source, $\mathcal{S}_i$, will have an associated position vector $\mathbf{r}_{\mathcal{S}_i}$, unit length orientation vector $\hat{\mathbf{n}}_{\mathcal{S}_i}$, power $P_{\mathcal{S}_i}$ and uniaxial symmetric, with respect to

$\hat{\mathbf{n}}_{\mathcal{S}_i}$, Lambertian radiation intensity profile $R(\phi)$ given by

$$R(\phi) = \frac{n+1}{2\pi} P_{\mathcal{S}_i} \cos^n(\phi) \qquad \text{for } \phi \in [-\pi/2, \pi/2] \tag{1}$$

Where the mode number, $n = 1$, for a pure Lambertian diffuser, such as the ceiling, and $n > 1$ for a diffusion spot from an LED with higher directionality.

For a given environment, we model the existence of $J = 1024$ identical single element receivers $\mathcal{R}_j$, uniformly distributed over the width x, length y, at a height $z = 1$m. Each receiver has a position vector $\mathbf{r}_{\mathcal{R}_j}$, orientation vector $\hat{\mathbf{n}}_{\mathcal{R}_j}$, active optical collection area $A_{\mathcal{R}_j}$ and a field of view $\text{FOV}_{\mathcal{R}_j}$ defined as the maximum uniaxial symmetric incident angle of radiation with respect to $\hat{\mathbf{n}}_{\mathcal{R}_j}$, that will generate a current in the photodiode.

Under the assumption that all surfaces exhibit Lambertian reflection characteristics, we follow the technique described in [21], and partition all surfaces into L elements $\mathcal{E}_l$ with position $\mathbf{r}_{\mathcal{E}_l}$, orientation $\hat{\mathbf{n}}_{\mathcal{E}_l}$, and size $A_{\mathcal{E}_l} = 1/\Delta A^2(\text{m}^2)$, where ΔA is the desired number of elements per meter. A given element will sequentially behave, firstly as a receiver $\mathcal{E}_l^{\mathcal{R}}$ with a hemispherical FOV, for which we can determine the received power $P_{\mathcal{E}_l}$, and secondly as a source $\mathcal{E}_l^{\mathcal{S}}$, with a radiation intensity profile $R(\phi)$ as given by (1) setting $n = 1$ and $P_{\mathcal{S}_i} = \rho_{\mathcal{E}_l} P_{\mathcal{E}_l}$, where $\rho_{\mathcal{E}_l}$ is the reflectivity of the element.

2.2. Impulse Response Calculations

The IR radiation incident upon a receiver $\mathcal{R}_j$ will be the result of the radiation emitted from a source $\mathcal{S}_i$ that has propagated directly through an unobstructed LOS path, and/or from the radiation that has undergone a finite number, k, reflections off the surfaces within the environment. It is also known [21, 15] that, for an intensity modulation, direct detection (IM/DD) channel, where the movement of transmitters, receivers or objects in the room is slow compared to the bit rate of the system, no multipath fading occurs, and, as such, can be deemed an LTI channel. The impulse response $h(t; \mathcal{S}_i, \mathcal{R}_j)$ is given by [21, 22]

$$h(t; \mathcal{S}_i, \mathcal{R}_j) = \sum_{k=0}^{k} h^k(t; \mathcal{S}_i, \mathcal{R}_j) \tag{2}$$

where $h^k(t; \mathcal{S}_i, \mathcal{R}_j)$ is the impulse response of the system for radiation undergoing k reflections between $\mathcal{S}_i$ and $\mathcal{R}_j$.

To determine the impulse response, we assume our source $\mathcal{S}_i$ emits a unit impulse at $t = 0$, i.e setting $P_{\mathcal{S}_i} = 1$W, then the LOS ($k = 0$) impulse response is given by the scaled and delayed Dirac delta function

$$h^0(t; \mathcal{S}_i, \mathcal{R}_j) \approx R(\phi_{ij}) \frac{\cos(\theta_{ij}) A_{\mathcal{R}j}}{D_{ij}} V(\frac{\theta_{ij}}{\text{FOV}_{\mathcal{R}j}}) \delta(t - \frac{D_{ij}}{c}) \tag{3}$$

Where, referring to figure 1, $D_{ij} = ||\mathbf{r}_{\mathcal{S}_i} - \mathbf{r}_{\mathcal{R}_j}||$ is the distance between source and receiver, and c is the speed of light. ϕ_{ij} and θ_{ij} are the angles between $\hat{\mathbf{n}}_{\mathcal{S}_i}$ and $(\mathbf{r}_{\mathcal{R}_j} - \mathbf{r}_{\mathcal{S}_i})$,

and between $\hat{\mathbf{n}}_{\mathcal{R}_j}$ and $(\mathbf{r}_{\mathcal{S}_i} - \mathbf{r}_{\mathcal{R}_j})$, respectively. $V(x)$ represents the the visibility function, where $V(x) = 1$ for $|x| \leq 1$, and $V(x) = 0$ otherwise.

For radiation undergoing $k > 0$ bounces, the impulse response is given by

$$h^k(t; \mathcal{S}_i, \mathcal{R}_j) = \sum_{l=1}^{L} h^{(k-1)}(t; \mathcal{S}_i, \mathcal{E}_l^{\mathcal{R}}) * h^0(t; \mathcal{E}_l^{\mathcal{S}}, \mathcal{R}_j) \tag{4}$$

Where $*$ denotes convolution, and the $k-1$ impulse response $h^{(k-1)}(t; \mathcal{S}_i, \mathcal{E}_l^{\mathcal{R}})$ can be found iteratively [22] from

$$h^k(t; \mathcal{S}_i, \mathcal{E}_l^{\mathcal{R}}) = \sum_{l=1}^{L} h^{(k-1)}(t; \mathcal{S}_i, \mathcal{E}_l^{\mathcal{R}}) * h^0(t; \mathcal{E}_l^{\mathcal{S}}, \mathcal{E}_l^{\mathcal{R}}) \tag{5}$$

Where all the zero order ($k = 0$), responses in (4) and (5) are found by careful substitution of the variables in (3). The computational time required for calculation of the impulse response using this iterative method is proportional to k^2 [23], and we will firstly limit ourselves to the a third order impulse response ($k = 3$), and secondly change the segmentation resolution of the environment for each reflection, setting $\Delta A_1 = 20$, $\Delta A_2 = 6$ and $\Delta A_3 = 2$. It should also be noted that the resultant impulse response in (2) will result in the finite sum of scaled delta functions which need to undergo temporal smoothing by subdividing time into bins of width Δt, and summing the total power in each bin [21]. For this work, we assume a single time bin width of $\Delta t = 0.1$ns.

3. The Channel Model

For a nondirected IR channel employing IM/DD, a source $\mathcal{S}_i$, which emits an instantaneous optical power $X_i(t)$, will produce a instantaneous photocurrent $Y_{ij}(t)$ at receiver $\mathcal{R}_j$ with photodiode responsivity r_j, in the presence of an additive, white Gaussian shot noise $N_j(t)$, and can be modelled as the linear baseband system, given by [24]

$$Y_{ij}(t) = r_j X_i(t) * h(t; \mathcal{S}_i, \mathcal{R}_j) + N_j(t) \tag{6}$$

If all I sources $\mathcal{S}_i$ emit an identical signal waveform, $X_1(t) = X_2(t) = \ldots = X_I(t)$, but with individually scaled magnitudes, a_i, the instantaneous photocurrent at a given receiver $Y_j(t)$ is simply the summation of (6) for all sources

$$Y_j(t) = \sum_{i=1}^{I} (r_j a_i X_i(t) * h(t; \mathcal{S}_i, \mathcal{R}_j)) + N_j(t) \tag{7}$$

Furthermore, through channel linearity, and knowing that r_j is identical for all receivers, a set of scaling factors a_i may exist providing a solution to

$$\sum_{i=1}^{I} a_i h(t; \mathcal{S}_i, \mathcal{R}_1) \approx \sum_{i=1}^{I} a_i h(t; \mathcal{S}_i, \mathcal{R}_2) \approx \ldots$$
$$\ldots \approx \sum_{i=1}^{I} a_i h(t; \mathcal{S}_i, \mathcal{R}_J) \tag{8}$$

Such that, by incorporation into (7), all of the J receivers will attain the same or very similar photocurrents

$$Y_1(t) \approx Y_2(t) \approx \ldots \approx Y_J(t) \tag{9}$$

Inspection of equations (7) to (9), implies a solution may require some scaling factors of ≤ 1, lowering the total received power, compared to if all sources were maximal. Furthermore, solving (9) for different environments, will yield non-identical sets of scaling factors, implying that the magnitude of received power, although equal at all locations within, will be different.

Drawing parallels with the IEEE 802.11a WiFi physical layer specification, that incorporates multi-rate transmission of up to 54Mbit/s [25], and recent work on rate-adaptive transmission [26] in the IR domain, if it is found that several environments have different received powers, the following method can be applied. Firstly, by normalising the I scaling factors, the equality result of (9) is independent of receiver power magnitude, and secondly, for different environments, we can adjust for example, the pulse characteristic, in order to increase or decrease the received power to make the power distributions equal. This then allows for the same optimal receiver design to be used in different environments, albeit under the compromise of variable data rates in the same manner as most other variable data rate systems.

To illustrate the final problem simplification we have applied, consider for example an environment, with dimensions $x = 6\text{m}, y = 6\text{m}, z = 3\text{m}$. In calculating a third order reflection impulse response ($k = 3$), the longest time of flight for the radiation to travel is $t = (4(6^2+6^2+3^2)^{0.5})/c \approx 120\text{ns}$, when it undergoes a path reflecting off the opposite corners of the room. Using an impulse response bin width $\Delta t = 0.1\text{ns}$, would produce 1200 samples for each impulse response train, for every combination of I sources and J receivers in (8).

Proposing a GA that can solve (8) for the possibly infinite number of source and transmitter configurations would be too unwieldy. By replacing the need to evaluate each bin of the impulse response train, with the need to find only the scaling factor solution for the time integral or DC value of the frequency response $H(0; \mathcal{S}_i, \mathcal{R}_j) = \int_{-\infty}^{\infty} h(t; \mathcal{S}_i, \mathcal{R}_j)dt$, equation (8) reduces to

$$\sum_{i=1}^{I} a_i H(0; \mathcal{S}_i, \mathcal{R}_1) \approx \sum_{i=1}^{I} a_i H(0; \mathcal{S}_i, \mathcal{R}_2) \approx \ldots$$
$$\ldots \approx \sum_{i=1}^{I} a_i H(0; \mathcal{S}_i, \mathcal{R}_J) \tag{10}$$

The power distribution optimisation should not be achieved at the expense of bandwidth and RMS delay spread. As (10) only quantifies the total power received, not when the power was received, we will feed back the solution into the original system model to quantify the worst case bandwidth and RMS delay spread, defined as the smallest and largest values at any location within the room respectively. The RMS

delay spread can be found from the original impulse response using [27]

$$\sigma = \sqrt{\frac{\int_{-\infty}^{\infty}(t-\omega)^2 h^2(t)dt}{\int_{-\infty}^{\infty} h^2(t)dt}} \tag{11}$$

Where ω is defined as:

$$\omega = \frac{\int_{-\infty}^{\infty} t h^2(t)dt}{\int_{-\infty}^{\infty} h^2(t)} \tag{12}$$

4. The Genetic Algorithm

GAs should be considered as a general framework that needs to be tailored to a specific problem [28]. Our initial work [13], detailed justified the methodology used to adapt the representation, fitness function, selection, recombination and mutation sub-routines found in the so-called *canonical* GA. This work uses the same two GAs as before, so only a brief description will be provided.

Firstly, we allow the scaling factors $a_i \forall i \in \{1, \ldots, I\}$ to take on a value in the set $\{0, 0.01, \ldots, 1\}$, such that the search space $\Phi_g = \{0, 0.01, \ldots, 1\}^I$, will provide $|\Phi_g| = 101^I$ possible solutions [29]. We further define a population $\Psi(t)$ at time t, of μ solutions $\mathbf{a}_\nu = (a_1, \ldots, a_I) \in \Phi_g, \forall \nu \in \{1, \ldots, \mu\}$.

At time t, each solution $\mathbf{a}_\nu$, is evaluated by the fitness function, F, which, for the results presented here, is given by

$$F(\mathbf{a}_\nu) = 100 - \left(100\left(\frac{\max H(0;\mathbf{a}_\nu) - \min H(0;\mathbf{a}_\nu)}{\max H(0;\mathbf{a}_\nu)}\right)\right) \tag{13}$$

Where $\max H(0;\mathbf{a}_\nu)$ and $\min H(0;\mathbf{a}_\nu)$ are the maximum and minimum DC frequency responses for any receiver after application of the scaling factor solution $\mathbf{a}_\nu$ to the source powers. It can be seen that we are measuring the percentage change or deviation from the peak power in the room. A solution $\mathbf{a}_\nu$, whose source scaling factors produce a perfectly uniform power distribution, will have a fitness of 100%. Furthermore our global maximum optimal solution, $\hat{\mathbf{a}}_\nu$, is given by

$$\hat{\mathbf{a}}_\nu = \max_{\mathbf{a}_\nu \in \Phi_g} F(\mathbf{a}_\nu) \tag{14}$$

The primary objective of the selection operator is to emphasise the fitter solutions, such that they are passed onto the next generation [30]. We implement two selection routines, namely, stochastic uniform sampling (SUS), and tournament selection. SUS selection schemes assign a probability of selection, p_ν^{prop}, proportional to an individuals relative fitness within the population, and is given by

$$p_\nu^{\text{prop}} = \frac{F(\mathbf{a}_\nu)}{\sum_{\nu=1}^{\mu} F(\mathbf{a}_\nu)} \tag{15}$$

The probabilities are then contiguously mapped onto a wheel, such that $\sum_{\nu=1}^{\mu} p_\nu^{\text{prop}} = 1$. Following the mapping, μ uniformly spaced numbers in the range $[0, 1]$ are offset by a singularly generated random number. Solutions for which the cumulative

probability spans any of the μ numbers is selected for reproduction [31], and for SUS selection we set $\mu = 200$.

Tournament selection is carried out by first ranking all solutions in the population $\Psi(t) = \{\mathbf{a}_1, \ldots, \mathbf{a}_\mu\}$ by their absolute fitness, where $\mathbf{a}_1$ is the fittest, and $\mathbf{a}_\mu$ is the least. Then, μ times, q solutions are randomly selected for a tournament, where the fittest is selected for the next generation. The probability of a solution $\mathbf{a}_\nu$ being selected is given by [30]

$$p_\nu^{\text{torn}} = \frac{1}{\mu^q}\left((\mu - \nu + 1)^q - (\mu - \nu)^q\right) \tag{16}$$

For the work presented, our tournament selection is carried out with $q = 3$, and a population size $\mu = 100$.

The reason for evaluating two selection routines is based on the transmitter hardware requirements. Tournament selection does not require proportional fitness assignments as in (15), and uses a lower population reducing the memory overhead. However, tournament selection is considerably more exploitative in nature, losing 50% of the solutions through the selection process alone [32], possibly finding a non-optimal solution. Results from both selection routines are presented to illustrate the difference in channel control performance.

Crossover imitates the principles of natural reproduction, and is applied with a probability, $\rho_c = 0.7$ to randomly selected individuals chosen by the either of the selection routines. Both algorithms apply double point, $m = 2$ crossover, that was implemented by generating two unique random integers in the range $\{1, \ldots, I-1\}$, that are subsequently sorted into ascending order, followed by simply exchanging the substrings between the successive cross over points.

Mutation was originally developed as a background operator [28], able to introduce new genetic material into the search routine such that the probability of evaluating a solution in Φ_g will never be zero. Mutation is performed on each individual scaling factor, $a_i \in \mathbf{a}_\nu \forall \nu \in \{1, \ldots, \mu\}$, with a probability $\rho_m = 0.05$ for SUS and with $\rho_m = 0.1$ for the tournament selection. If a given scaling factor a_i is chosen for mutation, it is simply replaced with another randomly generated number in the set $\{0, 0.01, \ldots, 1\}$.

Some feedback loop must exist that passes back information regarding the effectiveness of a solution at each generation. Presently the simulation will simply return the DC gain at each receiver location to the fitness function. In a practical system we envisage two methods. Firstly the receiver, or more precisely transceiver, returns the DC gain or SNR using a supervisory audio tone similar to GSM techniques, or secondly, if this optimisation process has been simulated on many scenarios, and the best and worst case powers are known, the transceiver could simply return a 'too high' or 'too low' command, informing the transmitter some change should be made to the ratios. Either method could be applied as and when needed, or within some predefined protocol space, and would be suitable when one or many receivers are present. Moreover, both methods are applicable when users enter or leave the room, since in theory, they too have the same receiver design that requires the same power distribution to operate.

In general, a GA is run over many generations until the algorithm converges, or the result has satisfied some defined solution criteria. Based on previous work [13], 5000 generations were suitable and applied to both algorithms. Furthermore due to the stochastic nature of the GA, for each simulation the results were inevitably slightly different, meaning that, to allow presentation of results that are both representative of the GAs performance, we conducted each simulation 30 times, such that each performance value presented within section 5 is the average after the 30 retrials.

5. Results

5.1. Receiver Alignment

To illustrate briefly the issue regarding the receiver alignment of a single element receiver in a MSD environment, consider an empty room with width $x = 6$m, depth $y = 6$m and height $z = 3$m. The ceiling and walls have a reflectivity $\rho = 0.75$, whilst the floor has a reflectivity $\rho = 0.3$. Upon the ceiling, 25 uniformly-distributed diffusion spots are formed, and, in the centre of the room at a height of $z = 1$m, a single element receiver with a $\text{FOV}_{\mathcal{R}} = 55°$, and active collection area of $A_{\mathcal{R}} = 0.0001\text{m}^2$, is present. Referring to figure 3 (a), the receiver is initially orientated vertically upwards, i.e along the z axis, and then rotated through $\pm 90°$ in both the x and y axis. The resultant received power, bandwidth and RMS delay spread can be seen in figure 2, where, with particular importance to the following discussion, the received power varies between 19.5μW and 58μW, equating to a 38.5μW or 66% power deviation, purely from the effects of alignment. Furthermore, the bandwidth is shown to vary between 12MHz and 61MHz, whilst the RMS delay spread varies between 1.1ns and 3.7ns. This result is purely based on one receiver with a given FOV at one location in one environment. Receivers in different positions will have their own rotational received power distribution. Additionally, taking into account the presence of many receivers that can be independently orientated, the problems an OW system designer faces become apparent.

5.2. Receiver Alignment and FOV

Section 5.1 provided results for a $\pm 90°$ rotation in both x and y axis, but gave no regard for what could be assumed to be typical user alignment behaviour. Five normal distributions with a mean $\bar{z} = 0$, (no rotation) and standard deviations $\sigma = \{7.8, 11.7, 19.5, 27, 35\}$, provided a respective 0.8 probability of rotational within $\pm\{10, 15, 25, 35, 45\}°$, and 0.99 within $\pm\{20, 30, 50, 70, 90\}°$ from the unrotated case. Each axis rotation in x and y was treated independently, but distributions were not mixed, such that for example there was a 0.64 chance of both axis's resulting in a rotation within $\pm 25°$, but scenarios that allowed for the x axis to rotate with a probability of 0.8 within $\pm 15°$ and the y axis to rotate with a probability of 0.8 within $\pm 45°$ were not investigated.

Using our established environment and receiver design, but where 1024 receivers are uniformly distributed over the room at a height of $z = 1$m, with alignment statistics based upon the normal distribution with $\sigma = 11.7$, the received power distribution, bandwidth and RMS delay spread can be seen in figures 4 (a),(c) and (e). The interesting point with the power received power distribution is the 'roughness' formed by the varying alignment at each receiver location, which causes the power to range between 20μW and 56.7μW, equating to a difference of 36.7μW, or approximately 65% power deviation. The bandwidth varies between 14.6MHz to 65.9MHz, and the RMS delay spread varies between 0.7ns to 2.1ns.

Applying the SUS GA to the diffusion spot intensities results in a received power distribution, bandwidth and RMS delay spread as shown in figures 4 (b),(d) and (f). The power deviation now ranges from 10.7μW to 18.7μW, equating to a difference of 8μW, or 43%. In comparison to the non optimised case, and defining the GA optimisation gain to be the improvement, as a %, in power deviation between the non optimised and optimised distributions, the GA optimisation gain for this scenario is 22%. Regarding bandwidth, the GA has reduced the peak bandwidth at a single location to 53.7MHz, but the worst case, or guaranteed minimum bandwidth remains the same at 14.6MHz. The peak, or worst case RMS delay spread has increased from 2.1ns to 2.7ns, a reasonable compromise, given the reduced power deviation the GA has provided.

Figure 5 (a) shows the GAs optimisation gain dependency on both FOV and receiver alignment distribution for the configuration described above, where, in the figure, the 80% angle defines to the normal distribution used to form a 0.8 rotational probability of a single axis being within $\pm\{10, 15, 25, 35, 45\}^\circ$ of the unrotated case. The 80% angle = 0 defines all receivers being vertically orientated. Figure 5 (b) shows the associated worst case bandwidth and RMS delay spread after the GA optimisation, clearly showing a correlation between lower bandwidth and larger RMS delay spread as the users 80% angle increases. It can be seen that the GA provides little gain for a receiver with FOV = 35°, when the user is statistically likely to align the receiver beyond ±10° from the vertical in either axis. Conversely, a receiver with FOV = 65° allows the GA to provide at least 17% gain up to an 80% angle of ±25°, but a bandwidth penalty is incurred above an 80% angle of ±15°, and the RMS delay spread is highest for lower 80% angles, where the user should statistically spend most of the time. Considering a receiver with a FOV = 45°, an optimisation gain can be achieved of between 21% and 25%, up to an 80% angle of ±10° with negligible impact on bandwidth and RMS delay spread. There is an argument for using either FOV, but care must be taken in balancing the tradeoff in GA optimisation gain, the users 80% rotation angle and the bandwidth and RMS delay spread penalties. For the remainder of the work presented, a receiver FOV = 55° will be assumed, as the GA provides optimisation gain between 20% to 23% for user 80% angles of ±15°, in line with bandwidth penalty drop-off point, and negligible RMS delay spread penalty.

5.3. Receiver Alignment and User Movement

Within our established environment with 1024 uniformly distributed receivers with FOVs = 55°, we incorporate a user movement pattern of 9 discrete positions, as shown in figure 3 (b). We also consider the use of the second GA, based on the tournament 3 (T3) selection routine. Figure 6 (a) depicts the SUS and T3 optimised and non optimised power deviation at each movement position and when empty, whilst figure 6 (b) depicts the associated optimised bandwidth (OB), non optimised bandwidth (NOB), optimised RMS delay spread (Orms) and non optimised RMS delay spread (NOrms) when empty (/E), and with movement (/M).

When empty, the non optimised power deviation is 65%, which, by application of the SUS and T3 GAs, is reduced to 43% and 46%, equating to a gain of 22% and 19% respectively. This result is also consistent with previous work [13, 14], where the SUS outperformed T3 by a few %. When a user is moving through the room, when not optimised the user varies the deviation between 58% and 65%, or a 6% perturbation from when empty. With movement the SUS based GA reduced the power variation to between 40% and 46%, a gain of up to 22% from the non-optimised case, and with now only a perturbation of 4.6% from the optimised empty room. Using the T3 based GA, the power deviation varied between 44% and 48%, a gain of up to 19%, and reduced the perturbation to just 2.5% from if the room was empty. In terms of bandwidth, a penalty of 2.4MHz is incurred only by the use of T3 when empty, whilst an RMS delay spread penalty of less than 1.3ns is imposed through use of either algorithm.

Implementing a second room of the same dimensions but with the ceiling, south and west walls having reflectivity $\rho = 0.8$, east wall reflectivity $\rho = 0.6$, north wall reflectivity $\rho = 0.5$, and floor reflectivity $\rho = 0.3$, using a movement pattern shown in figure 3 (c), the power deviation, bandwidth and RMS delay spread values can be seen in figure 7. When empty, the non optimised deviation is 73%, which, by application of the SUS and T3 GAs, is reduced to 46% and 51% respectively, equating to a gain of 27% and 22% respectively. Influenced by user movement, when not optimised, deviation varies between 62% and 73%, or a 10% perturbation from when empty. With movement, the SUS-based GA reduced the power variation to between 44% and 50%, a gain of up to 26% from the non optimised case, and with a perturbation of 4% from the optimised empty room. Using the T3-based GA, the power deviation varied between 46% and 51%, a gain of up to 21%, and a perturbation of 4% from if the room was empty. Similarly to the first room, a bandwidth penalty of 2.4MHz is incurred only by the use of T3 when empty, whilst an RMS delay spread penalty is again less than 1.3ns, through use of either algorithm.

6. Conclusions

This paper has demonstrated the approach of using a GA controlled MSD transmitter, capable of optimising the received power distribution in multiple environments with

user movement and alignment variability. Relationships have been drawn between the effectiveness of GA channel optimisation and the receivers FOV, and statistical alignment probabilities. A gain of up to 27% can be achieved for empty rooms, whilst a gain of up to 26% can be achieved when users are moving. Furthermore, user movement has been shown to perturb the channel by up to 10%, which can be reduced to as little as 2.5% using the GA. The optimisation has also been achieved with negligible impact on the bandwidth and RMS delay spread, and overall the method has shown the possibility of providing a highly adaptable method of overcoming channel variability with a solution that reduces receiver complexity for deployment application where cost and mobility are preferable.

References

[1] Green R J, Joshi H, Higgins M D and Leeson M S 2008 Recent developments in indoor optical wireless systems *IET Commun.*, vol. 2, no. 1, pp. 3–10

[2] Hashemi H, Yun G, Kavehrad G, Behbahani F and Galko P A 1994 Indoor propagation measurements at infrared frequencies for wireless local area networks applications *IEEE Trans. Veh. Technol.* vol. 43, no. 3, pp. 562–576

[3] O'Brien D C, Katz M, Wang P, Kalliojarvi K, Arnon S, Matsumoto M, Green R J and S. Jivkova 2005 Short range optical wireless communications *Wireless World Research Forum*

[4] Djahani P and Kahn J M 2000 Analysis of infrared wireless links employing multibeam transmitters and imaging diversity receivers *IEEE Trans. Commun.* vol. 48, no. 12, pp. 2077–2088

[5] Ramirez-Iniguez R and Green R J 2005 Optical antenna design for indoor optical wireless communication systems *Int. J. Commun. Syst.* vol. 18, no. 3, pp. 229–245

[6] Lee D C M, Kahn J M and Audeh M D 1997 Trellis-coded pulse-position modulation for indoor wireless infrared communications *IEEE Trans. Commun.*, vol. 45, no. 9, pp. 1080–1087

[7] Uno H, Kumatani K, Okuhata H, Shirakawa I and Chiba T 1997 ASK digital demodulation scheme for noise immune infrared data communication *Wirel. Netw.*, vol. 3, no. 2, pp. 121–129

[8] Moreira A J C, Valadas R T and de Oliveira Duarte A M 1997 Optical interference produced by artificial light *Wirel. Netw.*, vol. 3, no. 2, pp. 131–140

[9] Dickenson R J and Ghassemlooy Z 2003 A feature extraction and pattern recognition receiver employing wavelet analysis and artificial intelligence for signal detection in diffuse optical wireless communications *IEEE Trans. Wireless Commun.*, vol. 10, no. 2, pp. 64–72

[10] Kirkpatrick S, Gelatt C D and Vecchi M P 1983 Optimization by simulated annealing *Science*, vol. 220, no. 4598, pp. 671–680

[11] Wong D W K, Chen G and Yao J 2005 Optimization of spot pattern in indoor diffuse optical wireless local area networks *Opt. Express*, vol. 13,no. 8, pp. 3000–3014

[12] Wen M, Yao J, Wong D W K and Chen G C K 2005 Holographic diffuser design using a modified genetic algorithm *Opt. Eng.*, vol. 44, no. 8, pp. 085801 1–8.

[13] Higgins M D, Green R J and Leeson M S A genetic algorithm method for optical wireless channel control *IEEE J. Lightwave Tech.* "to be published".

[14] Higgins M D, Green R J and Leeson M S 2008 Genetic algorithm channel control for indoor optical wireless communications in *ICTON 2008*, Athens, vol. 4, pp 189–192.

[15] Kahn J M, Krause W J and Carruthers J B 1995 Experimental characterization of non-directed indoor infrared channels *IEEE Trans. Commun.*, vol. 43, no. 2–4, pp. 1613–1623, Feb

[16] Yang H and Lu C 2000 Infrared wireless LAN using multiple optical sources *IEE Proc. Optoelectron.*, vol. 147, no. 4, pp. 301–307

[17] Jivkova S, Hristov B A and Kavehrad M 2004 Power-efficient multispot-diffuse multiple-input-

multiple-output approach to broad-band optical wireless communications *IEEE Trans. Veh. Technol.*, vol. 53, no. 3, pp. 882–889.

[18] O'Brien D C, Faulkner G E, Zyambo E B, Jim K, Edwards D J, Stavrinou P, *et al* 2005 Integrated transceivers for optical wireless communications *IEEE J. Sel. Topics. Quantum Electron.*, vol. 11, no. 1, pp. 173–183

[19] Pohl V, Jungnickel J and von. Helmolt C 2000 Integrating-sphere diffuser for wireless infrared communication *IEE Proc. Optoelectron.*, vol. 147, no. 4, pp. 281–285

[20] Komine T and Nakagawa M 2004 Fundamental analysis for visible-light communication system using LED lights *IEEE Trans. Consum. Electron.*, vol. 50, no. 1, pp. 100–107

[21] Barry J R, Kahn J M, Krause W J, Lee E A and Messerschmitt D G 1993 Simulation of multipath impulse response for indoor wireless optical channels *IEEE J. Sel. Areas Commun.*, vol. 11, no. 3, pp. 367–379

[22] Carruthers J B, Carroll S M and Kannan P 2003 Propagation modelling for indoor optical wireless communications using fast multi-receiver channel estimation *IEE Proc. Optoelectron.*, vol. 150, no. 5, pp. 473–481

[23] Carruthers J B and Kannan P 2002 Iterative site-based modelling for wireless infrared channels *IEEE Trans. Antennas Propag.*, vol. 50, no. 5, pp.759–765

[24] Carruthers J B and Kahn J M 1997 Modeling of nondirected wireless infrared channels *IEEE Trans. Commun.*, vol. 45, no. 10, pp. 1260–1268

[25] Haratcherev I, Taal J, Langendoen K, Lagendijk R Sips H 2005 Automatic IEEE 802.11 rate control for streaming applications *Wireless Commun. Mob. Comput.*, vol. 5, no. 4, pp. 421–437

[26] Garcia-Zambrana A and Puerta-Notario A 2003 Novel approach for increasing the peak-to-average optical power ratio in rate-adaptive optical wireless communication systems *IEE Proc. Optoelectron.*, vol. 150, no. 5, pp. 439–444

[27] Pakravan M R and Kavehrad M 2001 Indoor wireless infrared channel characterization by measurements *IEEE Trans. Veh. Technol.*, vol. 50, no. 4, pp. 1053–1073

[28] Bäck T, Hammel U and Schwefel H P 1997 Evolutionary computation: Comments on the history and current state *IEEE Trans. Evol. Comput.*, vol. 1, no. 1, pp. 3–17

[29] Rothlauf F 2005 *Representations for genetic and evolutionary algorithms*. Springer-Verlag Berlin

[30] Bäck T 1996 *Evolutionary algorithms in theory and practice : evolution strategies, evolutionary programming, genetic algorithms*. Oxford University Press

[31] Baker J E 1987 Reducing bias and inefficiency in the selection algorithm in *Proc. 2nd. Int. Conf. Genetic Algorithms and their Applications*. NJ, USA, pp. 14–21.

[32] Poli R 2005 Tournament selection, iterated coupon-collection problem, and backward-chaining evolutionary algorithms in *Foundations of Genetic Algorithms* pp. 132–155.

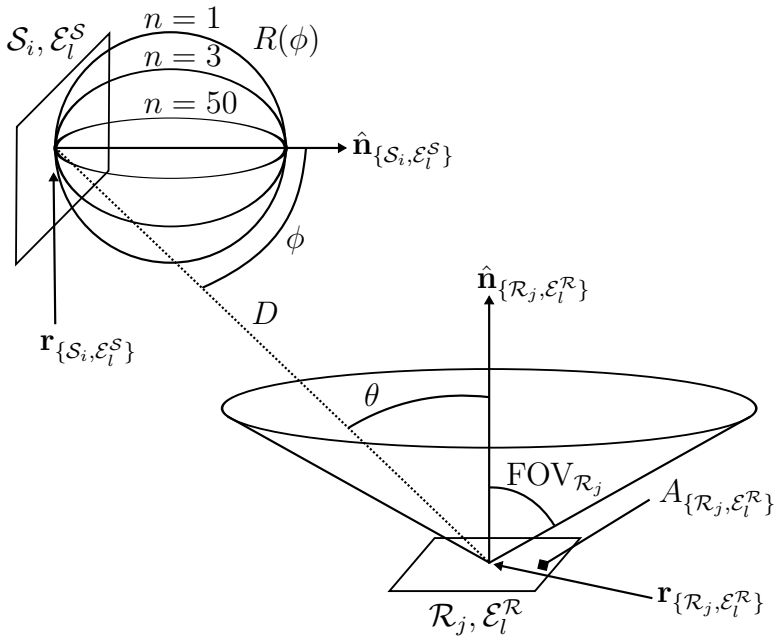

Figure 1. Source, receiver and reflector geometry, adapted from [21]

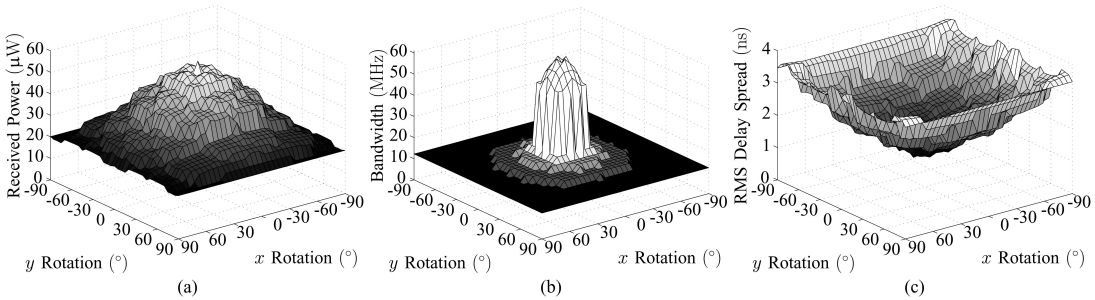

Figure 2. The angular dependence of: (a) Power, (b) Bandwidth and, (c) RMS delay spread.

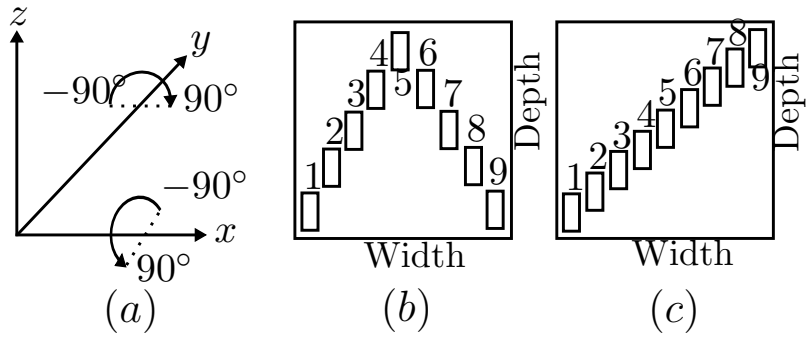

Figure 3. (a) Angle transformation system, (b) Movement pattern 1, (c) Movement pattern 2

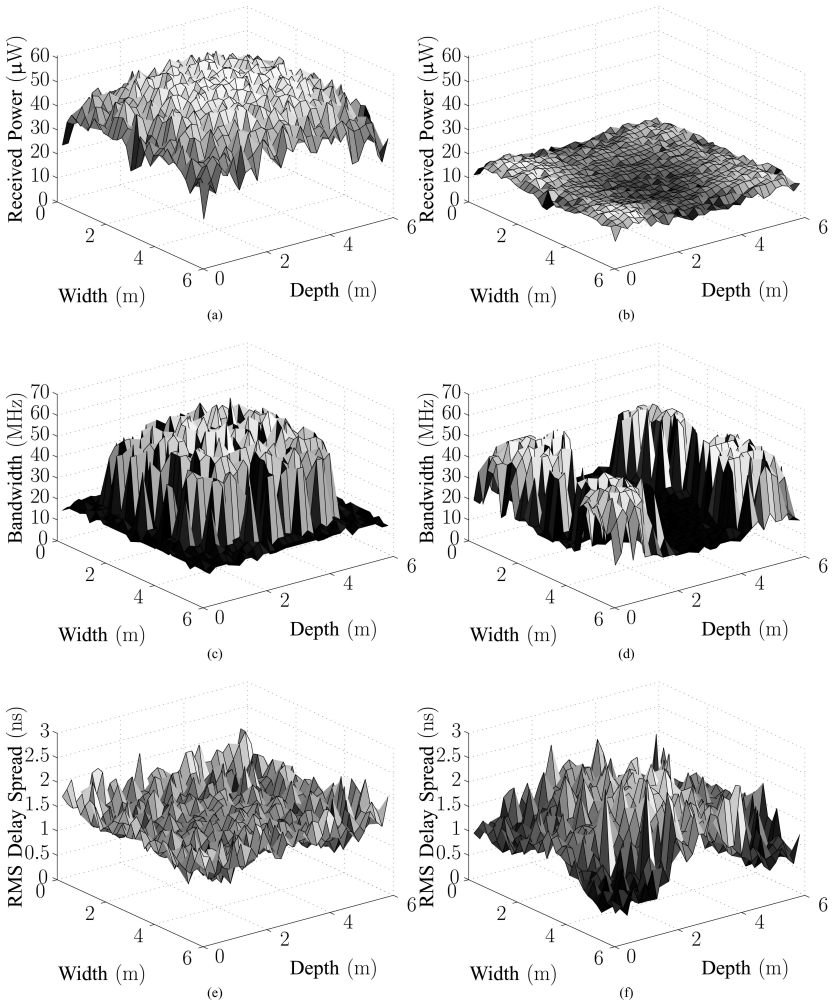

Figure 4. Empty room power, bandwidth and RMS delay spread. (a) Non Optimised power distribution. (b) Optimised power distribution. (c) Non optimised bandwidth. (d) Optimised bandwidth. (e) Non optimised RMS delay spread. (f) Optimised RMS delay spread.

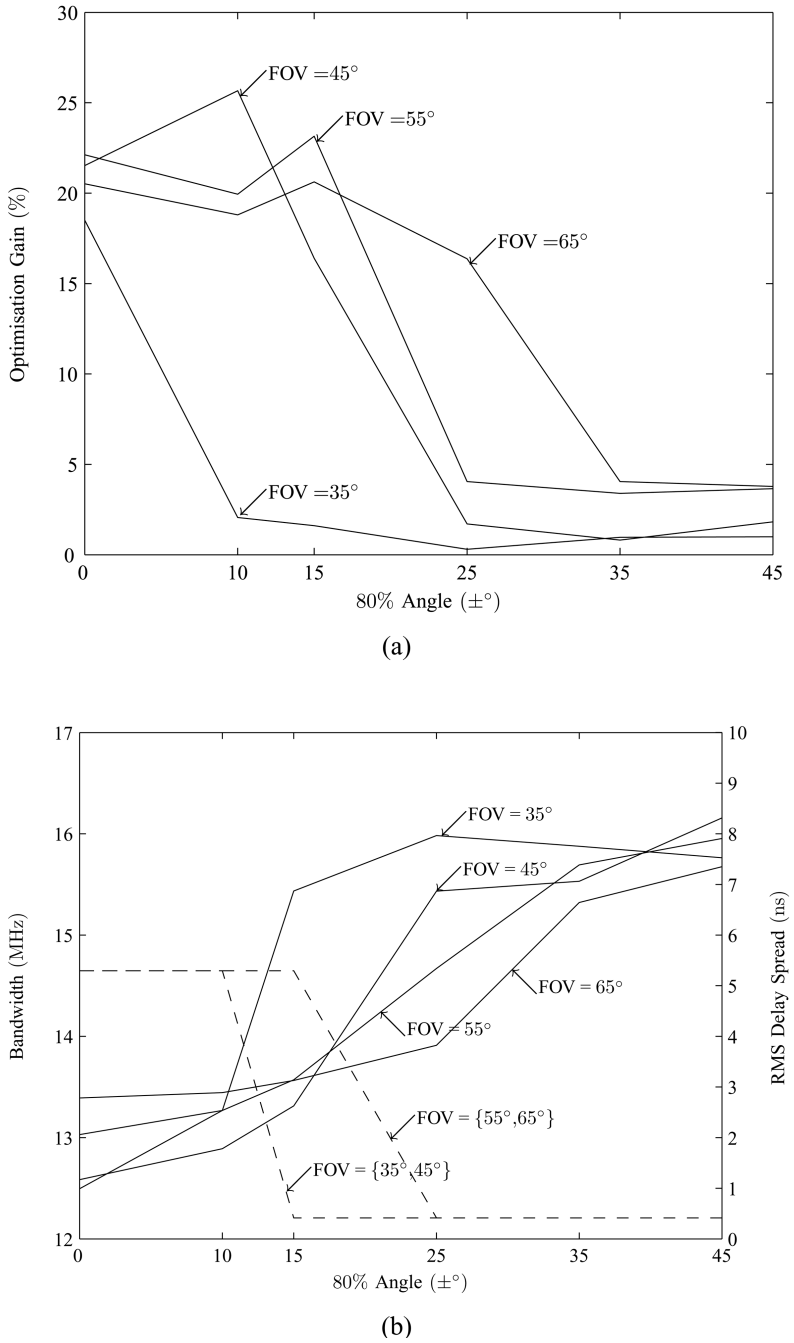

Figure 5. GA optimisation dependence on FOV and user alignment. (a) Optimisation gain. (b) Bandwidth (dashed) and RMS delay spread (solid).

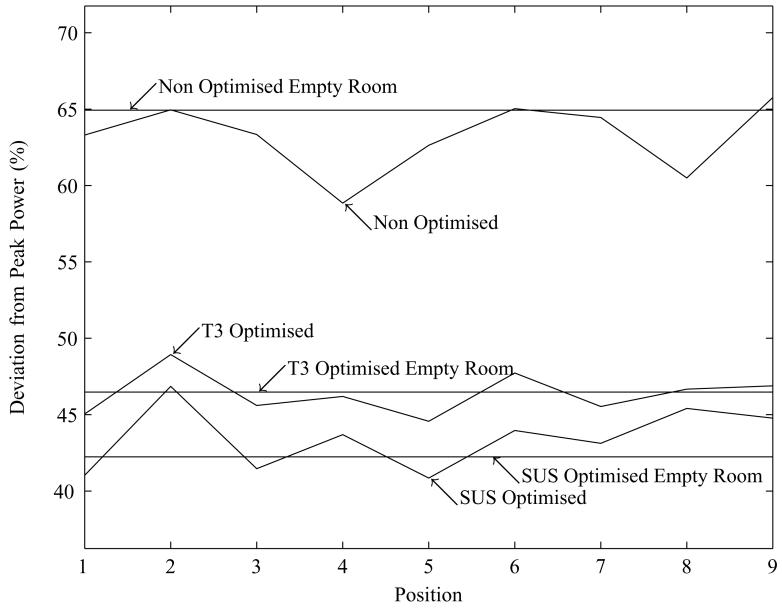

(a)

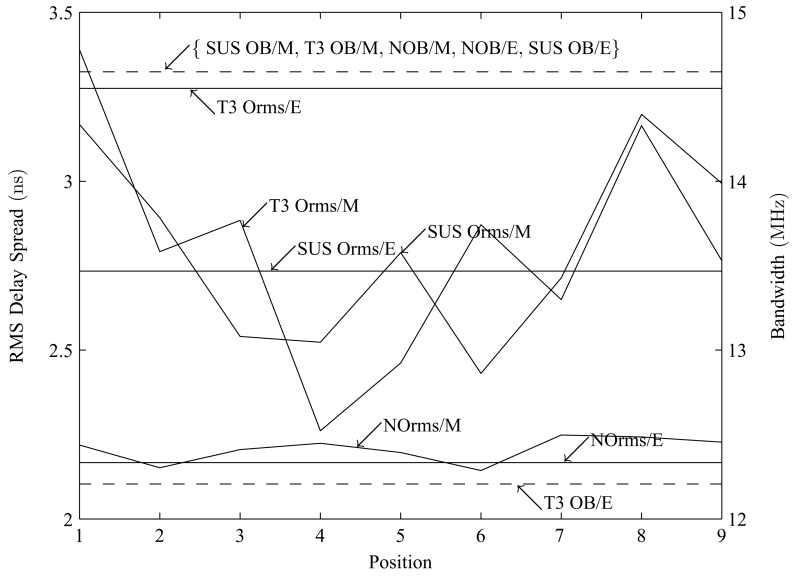

(b)

Figure 6. Environment 1, movement pattern 1. (a) Power deviation. (b) Bandwidth (dashed) and RMS delay spread (solid)

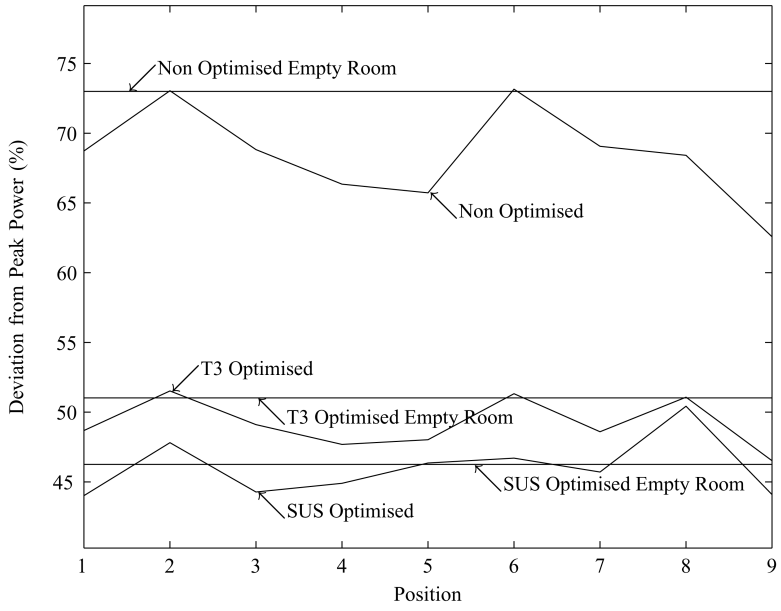

(a)

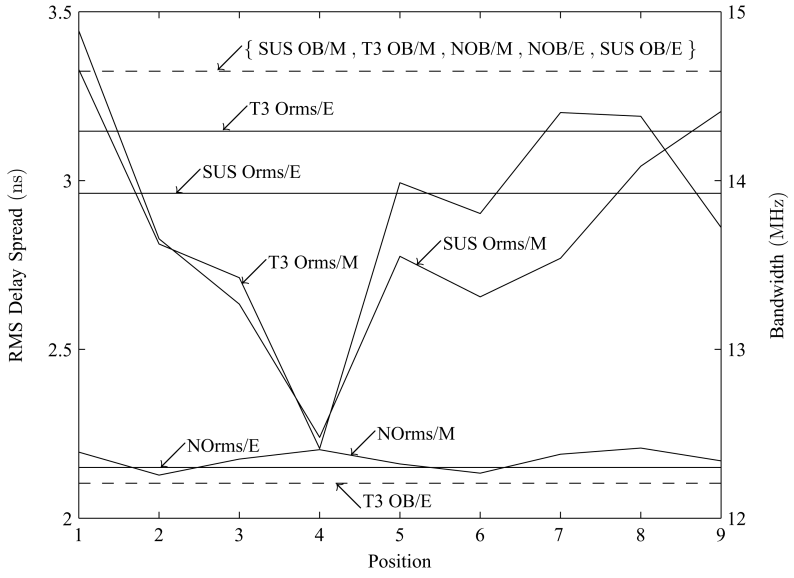

(b)

Figure 7. Environment 2, movement pattern 2. (a) Power deviation. (b) Bandwidth (dashed) and RMS delay spread (solid)